Solar Energy Materials & Solar Cells 96 (2012) 117–123

Contents lists available at SciVerse ScienceDirect

Solar Energy Materials & Solar Cells

journal homepage: www.elsevier.com/locate/solmat

Correlation between structure and photoluminescence of *c*-axis oriented nanocrystalline ZnO films and evolution of photo-generated excitons

Kun Gao [a], Qian Li [a], Zhigao Hu [b], Wenlei Yu [b], Jian Sun [a], Ning Xu [a], Jiada Wu [a,*]

[a] Key Laboratory of Micro and Nano Photonic Structures, Ministry of Education, Department of Optical Science and Engineering, Fudan University, Shanghai 200433, People's Republic of China

[b] Key Laboratory of Polar Materials and Devices, Ministry of Education, East China Normal University, Shanghai 200241, People's Republic of China

ARTICLE INFO

Article history:
Received 21 June 2011
Accepted 14 September 2011
Available online 1 October 2011

Keywords:
Zinc oxide
Nanocrystalline
Structure
Photoluminescence
Exciton

ABSTRACT

The structural and photoluminescent properties as well as the evolution of photo-generated excitons were studied in combination with the effects of thermal annealing for *c*-axis oriented nanocrystalline zinc oxide (nc-ZnO) films on Si (100) prepared by plasma assisted reactive pulsed laser deposition. The extra energy and the reactive oxygen species provided by ECR oxygen plasma result in the low-temperature *c*-axis oriented growth of nc-ZnO with wurtzite structure and low density of oxygen vacancies in the grown ZnO. The annealing process leads to the improvement of crystallinity and the growth of crystallites at the expense of the introduction of oxygen vacancies. The prepared nc-ZnO films emit strong near band edge (NBE) photoluminescence (PL) associated with longitudinal optical (LO) phonon replicas of free and bound excitons at 325 nm light excitation at 7 K. The temperature-dependent PL features reveal the evolution of radiative recombination processes with temperature and indicate that the room-temperature NBE luminescence is dominated by the LO phonon replicas of free excitons, whereas inappreciable visible emission in the room-temperature PL from as-deposited nc-ZnO suggests low-density oxygen vacancies in the samples.

1. Introduction

With a wide band gap of 3.37 eV and a large exciton binding energy of 60 meV at room temperature, zinc oxide (ZnO) is considered as an important material for optoelectronic devices such as short-wavelength light-emitting diodes, laser diodes, and detectors [1]. ZnO is also recognized as a promising solar energy material and has attracted much attention in photovoltaic applications. ZnO has a good transparency for the solar spectrum and can be used as a window layer in solar cells [2,3]. ZnO has an excellent conductivity and can be applied as a front conducting electrode in solar cells [4,5]. Due to its high electron mobility and almost equality in band gap energy with TiO_2, ZnO has been investigated as an alternative photoanode material for TiO_2 in dye-sensitized solar cells (DSSCs) [6–8]. ZnO has also been proposed to form type-II heterojunctions with other wide band gap II–VI semiconductors as an alternative structure for photovoltaic applications [9,10]. In addition to bulk and film materials, ZnO with various nanostructures is particularly attractive for photovoltaic devices. In the DSSCs constructed from nanocrystalline ZnO (nc-ZnO) films, dye excited states undergo rapid charge separation, with electrons injected into the nc-ZnO films and holes leaving the opposite side of the device. The replacement of a flat and smooth surface of ZnO back electrode by a rough nc-ZnO film is an effective approach to increase light path in solar cells [4]. The refractive index of nanostructured ZnO can be tailored by coating on an absorber surface. ZnO with varied refractive index suppresses the reflection at surface, and therefore can be used as a light coupling layer for antireflective coating as well as solar thermal selective surfaces in solar cells [11].

ZnO nanostructures can be synthesized by different methods using various liquid, gaseous, solid, and colloidal systems and their combinations as the precursor media for nanoscale assemblies. Among them, plasma-based methods using reactive gaseous precursors are versatile for the synthesis of nanostructured materials including various forms of ZnO nanostructures [12]. Despite the achievements in the preparation of ZnO nanostructures and the extensive studies of nanostructured ZnO, further work is necessary for the material to be used commercially, including the studies on the fundamental properties and their dependence on preparation approaches and treatment conditions. For photovoltaic applications, in particular, the centers and mechanisms responsible for the generation, transfer, and relaxation of photo-generated excitons as well as their correlation with structure need to be further clarified.

We have recently succeeded in the synthesis of highly *c*-axis oriented and hexagonal wurtzite structured nc-ZnO films by plasma

* Corresponding author. Fax: +86 21 65641344.
E-mail address: jdwu@fudan.edu.cn (J. Wu).

0927-0248/$ - see front matter © 2011 Elsevier B.V. All rights reserved.
doi:10.1016/j.solmat.2011.09.033

assisted reactive pulsed laser deposition [13,14]. An oxygen plasma ignited by electron cyclotron resonance (ECR) microwave discharge was used as a reactive oxygen source for the reactive deposition of nc-ZnO films on several kinds of substrates. In this paper, we present a systematic study on nc-ZnO films deposited on lattice mismatched Si(100) substrates, about the dependence of the structure and photoluminescence (PL) on annealing process and the correlation between the structural and the luminescent properties. Temperature dependent PL is also presented here for the examination of the transfer and relaxation of photo-generated excitons in the prepared nc-ZnO films.

2. Experimental section

2.1. Sample preparation

Nc-ZnO thin films were reactively deposited by oxygen plasma assisted pulsed laser deposition. A detailed description of the experimental equipment and the deposition procedure has been provided previously [13,14]. A metallic zinc target (99.999% in purity) was ablated by a pulsed laser beam in the environment of an oxygen plasma ignited by means of electron cyclotron resonance (ECR) microwave discharge in pure ($>99.999\%$) oxygen gas. The zinc plasma created by the zinc target ablation expanded in the oxygen plasma and the oxygen plasma was further excited by the laser induced zinc plasma during its expansion from the target to the substrate [15]. Polished n-type single crystalline Si (100) wafers were used as substrates after being chemically cleaned to remove surface contaminants and natural oxide layer. The substrate was positioned parallel to the target surface with a distance of 40 mm. The laser induced zinc plasma expanded reactively through the highly reactive oxygen plasma towards the substrate surface, resulting in the reactive deposition of nc-ZnO films at a temperature of about 80 °C. After deposition, the deposited nc-ZnO films were exposed to thermal annealing process at different temperatures in air for 30 min.

2.2. Sample characterization

Surface morphology of the prepared nc-ZnO films was examined by atomic force microscopy (AFM) with a scanning probe microscope (PSIA, XE-100), which worked in the AFM non-contact mode. The crystalline structure was analyzed by X-ray diffraction (XRD) with a Rigaku D/max-γB X-ray diffractometer in the θ–2θ configuration using the Ni-filtered Cu Kα radiation ($\lambda=0.15406$ nm). The structure of the films was also characterized by Raman scattering and Fourier transform infrared (FTIR) spectroscopy through the analysis of oxide phases and vibrational modes. The Raman scattering measurements were performed with a Jobin-Yvon LabRAM HR 800UV micro-Raman spectrometer using 325 nm laser beam from a He–Cd laser as the exciting light, while the FTIR spectra were recorded with a Bruker Vertex 80 V spectrometer. PL measurements were performed for the as-deposited and the annealed nc-ZnO films by normally exciting the samples with 325 nm laser light from a CW He–Cd laser (Melles Griot, 3074-M-X04). The nc-ZnO samples were fixed to the cold holder of a closed-cycle refrigerator (Arscryo, DE-204) and cooled down to the desired temperature for measurements. The PL spectra were recorded by collecting the emitted luminescence at normal direction with a 0.5 m spectrometer (Acton Research, Spectra Pro 500i) and an intensified charge-coupled device (ICCD) (Andor Technology, iStar DH720), which was attached to the exit port of the spectrometer.

3. Results and discussion

3.1. Surface morphology

The prepared nc-ZnO films have good adhesion to the substrates. The examination of surface morphology by AFM reveals that the prepared films exhibit a smooth surface appearance with an average root mean square value of roughness of about 1.0 nm over 1 μm × 1 μm surface area. AFM images of the as-deposited and the annealed nc-ZnO films on Si (100) substrates have been presented elsewhere [13,14]. No significant influence on the surface morphology by post deposition annealing has been observed.

3.2. Crystal structure

XRD characterization reveals that the as-deposited nc-ZnO films are of wurtzite structure with a preferred orientation along the *c*-axis perpendicular to the substrate surface. Curve 1 in Fig. 1 is a typical XRD pattern taken from an as-deposited nc-ZnO film with a thickness of about 80 nm. Besides the strong and sharp peak ($2\theta=69.14^\circ$) attributed to the diffraction from the Si substrate, the dominant peak is identified as the (002) diffraction of wurtzite ZnO phase. The oriented crystallographic growth of ZnO is partially due to the extra energy provided by the plasma stream to the precursors arriving at the surface, which promotes the reaction rate at the surface and enhances the mobility of the arrived precursors, hence facilitating the oriented growth of the crystalline film at low temperatures. Several weak peaks, also indexed to the hexagonal wurtzite structured ZnO, can be observed in addition to the (002) diffraction, indicating the presence of orientations other than the dominant *c*-axis orientation. It is noted that 2θ value corresponding to the (002) diffraction is 33.70°, much smaller than 34.422°, the standard value for bulk ZnO (JCPDS: 36-1451), suggesting the imperfection of the ZnO wurtzite structure. Meanwhile, the full width at half-maximum (FWHM) of the (002) peak is rather large (~0.85°), revealing the small size of the ZnO crystallites. From the diffraction angle and the FWHM of the (002) peak, the mean size of the prepared ZnO crystallites in this film is calculated to be about

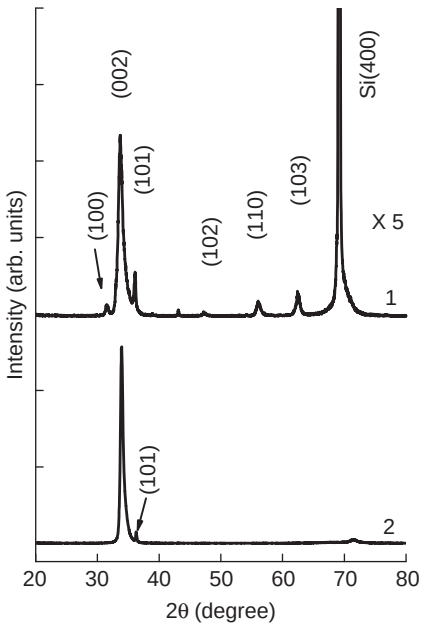

Fig. 1. XRD patterns of as-deposited nc-ZnO films on Si: (1) with a thickness of 80 nm and (2) with a thickness of 500 nm. Pattern 1 shown in the figure is magnified by 5 vertically.

10 nm using the Scherrer's formula [16]:

$$d = \frac{K\lambda}{\beta \cos\theta},$$

where d is the mean diameter of the crystallites, and K, λ, β, and θ the Scherrer parameters ($=0.9$ generally), X-ray wavelength (0.15406 nm here), FWMH of the diffraction peak, and Bragg diffraction angle, respectively. Using the well-known x-ray diffraction formula for a hexagonal structure [17], the lattice constants are determined to be $a=0.531$ nm and $c=0.325$ nm from the XRD data.

As the films grow thicker up to about 300 nm, the intensity of these weak diffraction peaks decreases while that of the dominant (002) diffraction increases, together with the peak position shifting towards larger angles and the peak width narrowing gradually. Above 300 nm, these weak diffraction peaks become almost indiscernible and the features of XRD pattern remain almost unchanged. Unless otherwise specified, the present work was mainly performed for the films with a thickness of about 500 nm. The XRD pattern obtained for an as-deposited nc-ZnO film with a thickness of 500 nm is also depicted in Fig. 1 (curve 2). It can be seen that the (002) diffraction peak of wurtzite ZnO dominates the XRD pattern, except a very weak peak indexed to ZnO (101). This XRD pattern suggests the nearly oriented crystallographic growth of the nc-ZnO films with the c-axis perpendicular to the substrates. However, the 2θ value corresponding to the (002) diffraction is still smaller than the standard value for bulk ZnO, suggesting that there is some stress in the as-deposited films. On the other hand, narrowing of the (002) peak reveals that the crystallites grow larger in size during the growth of the film. The calculated lattice constants of the nc-ZnO structure and the determined mean size of the crystallites are listed in Table 1 together with the measured XRD data.

After annealing in air, the (002) peak is observed to shift towards the larger diffraction angles along with a narrowing in the diffraction peak, implying that the stress in the film was released and the crystallites grew larger during thermal annealing. A gradual shift in diffraction angle and a gradual narrowing in diffraction peak with annealing temperature illustrated in Fig. 2 clearly reveal the progressive improvement in nc-ZnO crystallinity. In addition, the orientation of the crystallinity was also improved by thermal annealing, as revealed by the disappearance of the (101) peak, which is only observed from the as-deposited and the low-temperature annealed films. After annealing at temperatures above 500 °C, the (101) diffraction can no longer be recognized. The peak positions and the FWHMs of the (002) diffraction peak of the nc-ZnO films after annealing at different temperatures are tabulated in Table 1. The positions of the weak (101) peak of the as-deposited and the low-temperature annealed films are also listed in the table. Using the x-ray diffraction formula and the Scherrer's formula, the lattice constants of the wurtzite structure and the mean size of the crystallites in the films are determined for the nc-ZnO films after annealing at different temperatures, as tabulated also in Table 1. It can be seen that the crystallites in the nc-ZnO films grew larger with annealing temperature. With respect to crystallinity, however, temperatures around 700 °C are most appropriate: no diffractions other than the (002) one could be observed from the film after annealing above 600 °C, indicating the high c-axis orientation; the films after annealing at temperatures from 600 to 800 °C have the (002) diffraction and lattice constants very close to the standard values for bulk wurtzite ZnO.

3.3. Oxide phase and vibrational modes

FTIR measurements confirm the formation of wurtzite ZnO phase in the prepared films. Theoretical calculation has predicted the Zn–O bond excitation around a wavenumber of 410 cm^{-1} for high quality ZnO, while ZnO usually shows distinct absorption bands around 460 cm^{-1} [18–20]. Fig. 3 illustrates the recorded FTIR transmission spectra in the wavenumber region below 1500 cm^{-1} for the as-deposited film on Si and the films after annealing at different temperatures, together with that recorded for the Si substrate as a reference. In addition to the absorptions originating from the substrate, a strong absorption is clearly observed at about 420 cm^{-1} for the prepared films whether annealed or not. This band is due to zinc oxide and can be attributed to Zn–O vibrational modes. It is also observed that this absorption becomes stronger and the absorption band gets much narrower after annealing, indicating the improvement in crystallinity resulting from post deposition annealing, consistent with the results obtained by XRD characterization. Furthermore, a weak but distinct absorption near 570 cm^{-1} appears as a shoulder in the spectrum taken from the as-deposited film (marked by an asterisk in the figure). This absorption

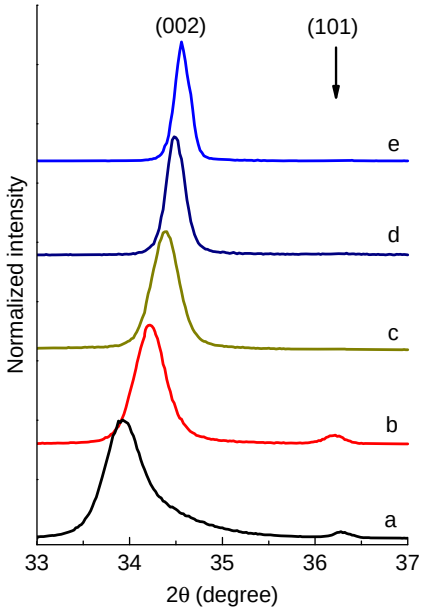

Fig. 2. Detailed XRD patterns of (002) diffraction peaks showing diffraction shift and peak narrowing: (a) as-deposited; (b) annealed at 400 °C; (c) annealed at 600 °C; (d) annealed at 800 °C; and (e) annealed at 1000 °C. The weak (101) peaks also appear in the XRD patterns obtained from the as-deposited film and the film annealed at 400 °C.

Table 1
Measured positions of (002), and (101) XRD peaks and FWHM of (002) peak, and calculated lattice constants and crystallite diameters.

Sample	As-deposited	Annealed at 400 °C	Annealed at 600 °C	Annealed at 800 °C	Annealed at 1000 °C
(002) peak position (2θ)	33.93°	34.22°	34.40°	34.48°	34.56°
(101) peak position (2θ)	36.20°	36.26°	Not identified	Not identified	Not identified
FWHM of (002) peak	0.51°	0.40°	0.34°	0.23°	0.18°
Lattice constant c (nm)	0.528	0.524	0.521	0.520	0.519
Lattice constant a (nm)	0.324	0.324	Not calculated	Not calculated	Not calculated
Crystallite diameter d (nm)	16	20	24	36	45

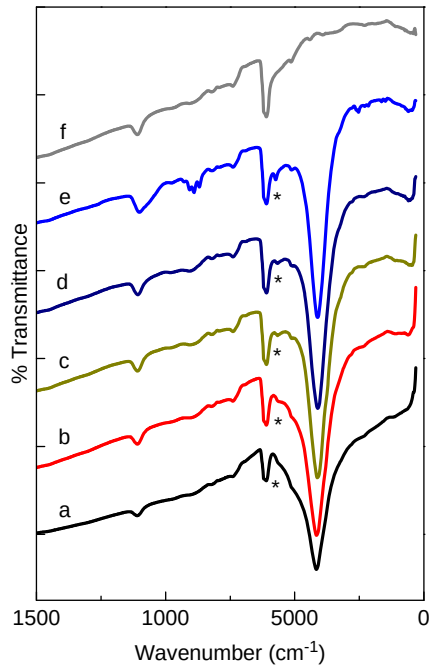

Fig. 3. FTIR transmission spectra of nc-ZnO films on Si: (a) as-deposited; (b) annealed at 400 °C; (c) annealed at 600 °C; (d) annealed at 800 °C; (e) annealed at 1000 °C; and (f) FTIR transmission spectrum of Si substrate as a reference.

is attributed to the polar A_1 mode with longitudinal optical (LO) phonons, which is both IR and Raman active. The A_1 (LO) mode has a high efficiency to be excited in Raman scattering and hence the Raman signal corresponding to the A_1 (LO) mode is easy to be observed. In contrast, this mode is usually hard to be observed in IR characterization [18–21]. In our case, this absorption can be identified in the FTIR measurements and becomes prominent after annealing, with its intensity increasing with an increase in annealing temperature, as clearly shown in Fig. 3.

Raman scattering measurements provide further evidence for the wurtzite ZnO phase in the prepared films. For hexagonal wurtzite ZnO, the phonon modes belonging to the E_2, E_1, and A_1 symmetries are Raman active [22]. Of them, the non-polar phonon modes with symmetry E_2 have two frequencies associated with oxygen and zinc sublattices, and the polar A_1 and E_1 modes split into LO and transverse optical (TO) components, respectively, exhibiting different frequencies. Therefore, there are six Raman active phonon modes E_2 (low), E_2 (high), A_1 (TO), A_1 (LO), E_1 (TO), and E_1 (LO) for wurtzite ZnO [23,24]. Fig. 4 shows a typical Raman spectrum recorded for the as-deposited film. The scattering signals are rather strong with more resolved peaks compared with our previous work [13,14]. This could be due to the stronger absorption of 325 nm light for sample excitation. The spectra exhibit three prominent peaks at 570, 1150, and 1730 cm^{-1} and several weak ones. Two Raman peaks corresponding to the E_2 (high) and the A_1 (LO) modes at 438 and 570 cm^{-1}, respectively, are observed as expected from the Raman selection rules in wurtzite crystal structure. Three weak features at 325, 655, and 998 cm^{-1} are also resolved (marked by asterisks in the figure). They could be attributed to multiple-phonon scattering processes [24,25]. It is worthwhile noting that the A_1 (LO) mode is remarkably strong, and the frequency shifts of the 2LO and 3LO phonons are also remarkably prominent. Intense multiple-phonon scattering processes of the A_1 (LO) modes have previously been observed in high quality ZnO bulk crystal materials [26]. Raman spectra recorded for the nc-ZnO films after annealing in the temperature range from 400 to 1000 °C are depicted in Fig. 5, along with those obtained from the as-deposited film for comparison. It can be seen from Fig. 5 that no

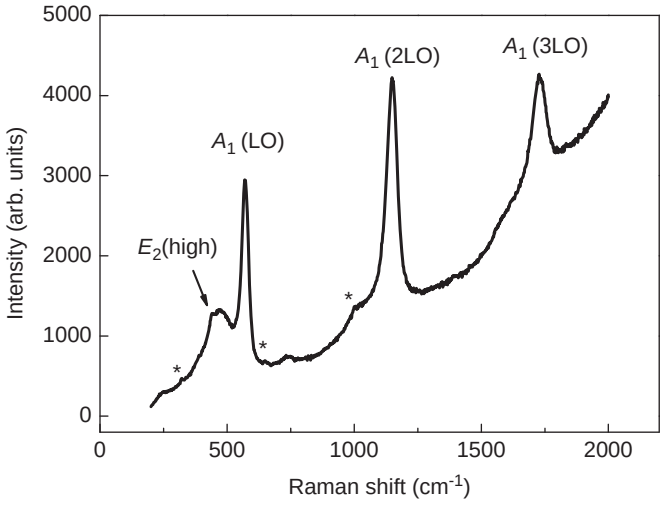

Fig. 4. Raman scattering spectrum of as-deposited nc-ZnO film on Si.

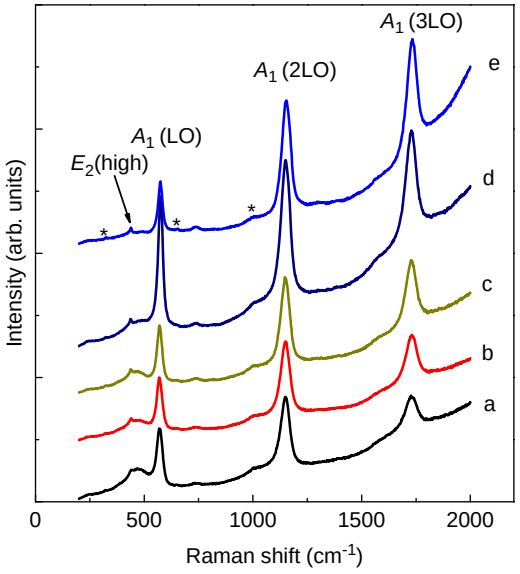

Fig. 5. Raman scattering spectra of nc-ZnO films on Si: (a) as-deposited; (b) annealed at 400 °C; (c) annealed at 600 °C; (d) annealed at 800 °C; and (e) annealed at 1000 °C.

obvious annealing effects are observed up to 600 °C, except that the E_2 (high) Raman peak becomes much resolved for the films after annealing compared with the as-deposited one. High-temperature annealed nc-ZnO films exhibit stronger Raman scattering signals. However, there seems no monotonic increase in Raman signals with annealing temperature and the strongest Raman signals are observed from the films after annealing at temperatures around 800 °C, most probably corresponding to the improvement in crystallinity resulting from annealing at about 800 °C.

3.4. Room-temperature photoluminescence

Fig. 6(a) illustrates the room-temperature (RT) PL spectrum taken from the as-deposited nc-ZnO films on Si substrates. At the excitation of light with a wavelength of 325 nm, the as-deposited nc-ZnO film emits strong UV luminescence peaking at 381.6 nm (3.249 eV). This UV PL is assigned to the room-temperature free exciton related near band edge (NBE) emission in ZnO, namely, the recombination of free excitons through an exciton–exciton

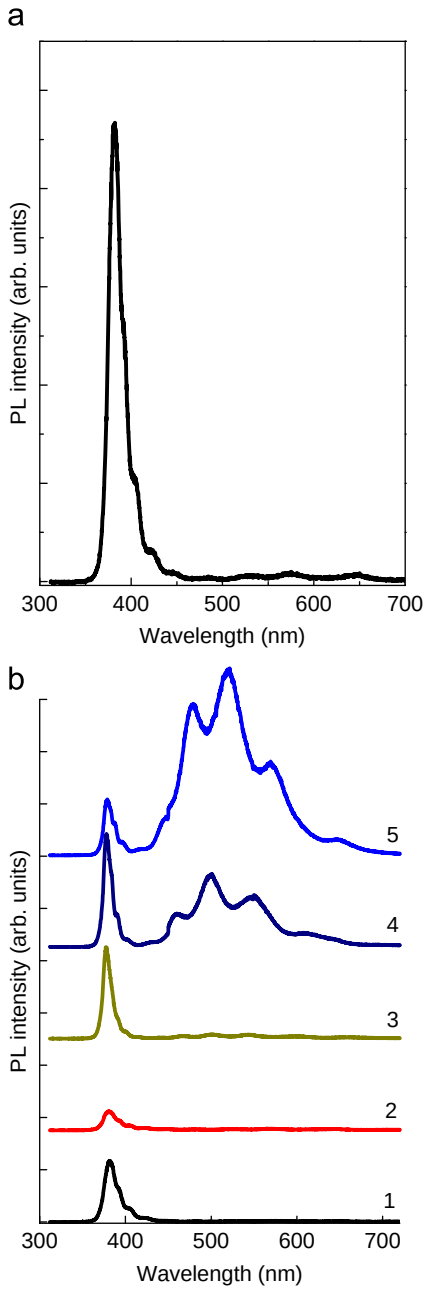

Fig. 6. (a) Room-temperature PL spectra of as-deposited nc-ZnO film on Si; (b) room-temperature PL spectra of as-deposited and annealed nc-ZnO films on Si: (1) as-deposited; (2) annealed at 400 °C; (3) annealed at 600 °C; (4) annealed at 800 °C; and (5) annealed at 1000 °C.

collision process [27,28], which is evidenced by temperature dependent PL measurement as will be described below. The NBE emission band of the as-deposited nc-ZnO film is rather broad and extends to 435 nm in the long wavelength side with an FWHM of about 20 nm. It can be seen that the intensity and feature of the NBE emission show a strong dependence on the annealing process, as shown by Fig. 6(b), which displays the RT PL spectra taken from the as-deposited and the annealed nc-ZnO films. For the nc-ZnO film annealed at 400 °C in air for 30 min, the intensity of the NBE emission decreases significantly. With the annealing temperature increasing above 400 °C, however, an enhancement in the NBE emission and a narrowing in the emission band are observed. The strongest NBE emission is observed for the films annealed at about 800 °C, whose NBE emission peaks at 377.8 nm and spans from 362 to 411 nm, or from 368 to 396 nm with an intensity above 10% of

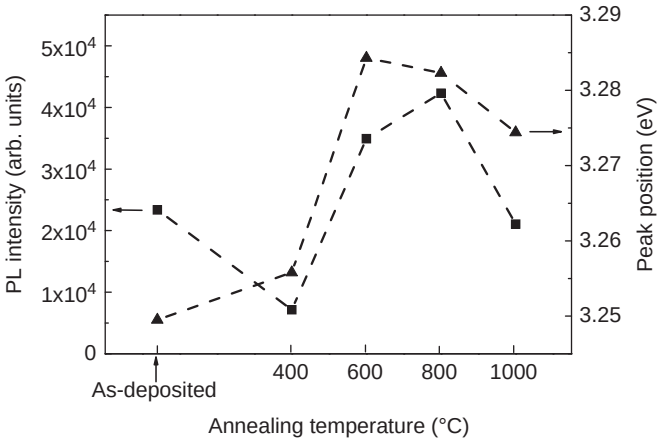

Fig. 7. PL intensity and peak position of as-deposited and annealed nc-ZnO films vs. annealing temperature.

the peak intensity, with its FWHM of approximately 10 nm. Further increasing the annealing temperature results in a decrease in the intensity of the NBE emission, as shown in Fig. 6. The wavelength of the emission peak is also observed to be dependent on annealing temperature. The dependence of the PL intensity and peak position of the NBE emission on annealing temperature is depicted in Fig. 7.

In addition to the NBE emission, green and other visible luminescence, usually observed in almost all ZnO prepared on different substrates by various methods [29–32], can hardly be detected in our case from the as-deposited film and the films after annealing below 600 °C, with the intensity less than 2% of the NBE emission intensity for the as-deposited film and less than 5% for the 600 °C annealed films. The visible photoluminescence of ZnO is related to the deep level defects, such as oxygen vacancies, oxygen interstitials and zinc interstitials in ZnO. Green emission in ZnO is generally explained by the radiative recombination of a photo-generated hole with the electron in a singly ionized oxygen vacancy [30,31], while yellow emission is attributed to oxygen interstitials [32]. Although the actual recombination mechanisms for visible emission are still not fully understood, the almost absence of the visible defect-related deep level (DL) emission from our as-deposited film and films after annealing below 600 °C reveals a lower density of such defects in the nc-ZnO films and a higher thermal stability of the prepared nc-ZnO films at temperatures as high as 600 °C. The low density of oxygen vacancies in our nc-ZnO films could be attributed to the ECR oxygen plasma, which provides the ZnO crystallites with sufficient reactive oxygen during the growth of nc-ZnO. However, it can be seen from Fig. 6 that with further increase in the annealing temperature, the DL emission is greatly enhanced, indicating the introduction of deep level defects such as oxygen vacancies during high temperature annealing. For the film annealed at 800 °C, i.e. the film having the highest efficiency for UV NBE emission at 325 nm light excitation, the intensity of the DL emission increases to be higher than half of that of the NBE emission. Much more intense DL emission is observed from the film after annealing at 1000 °C, whose DL emission is remarkably enhanced with its intensity more than three times that of the NBE emission. The intensity of the DL emission and the relative intensity of the DL emission to the NBE emission are plotted in Fig. 8 as functions of annealing temperature, together with the intensity of the NBE emission for reference.

3.5. Temperature dependent photoluminescence and photo-generated excitons

The above RT PL measurements show that the UV NBE luminescence from the nc-ZnO films is greatly enhanced after

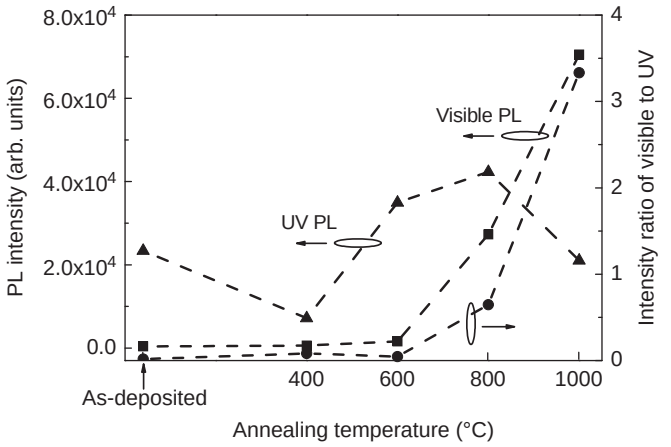

Fig. 8. Intensity dependence of NBE and DL emissions and their intensity ratio on annealing temperature.

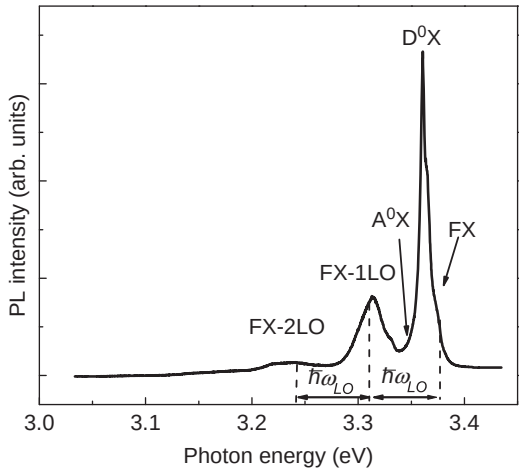

Fig. 9. Low-temperature PL spectrum of nc-ZnO film on Si after annealing at 600 °C. The PL spectrum was taken at 7 K.

annealing at around 600 °C while the DL luminescence remains very weak. The films thus prepared and annealed were submitted to various temperatures for temperature dependent PL measurements. At low temperatures, the NBE luminescence is dominated by radiative decays from a number of free and bound exciton complexes. Fig. 9 displays a typical high resolution PL spectrum taken at 7 K from the annealed nc-ZnO film. The details of the PL features related to the emissions with various excitons and their phonon replicas are shown in the figure. The emission at 3.360 eV with its FWHM of about 8 meV is the strongest in the spectrum. This strong and narrow emission peak is associated with bound excitonic emission at neutral donors (D^0X) [27,28]. The NBE luminescence extends to lower energies and the D^0X peak is accompanied by an emission at 3.346 eV, which can be attributed to the contribution of neutral-acceptor bound excitons (A^0X). At the high energy side of the D^0X peak, the emission associated with free excitons (FX) appears as a shoulder. In addition to the emissions associated with donor and acceptor bound excitons and that with free excitons, two PL bands are clearly resolved at 3.313 and 3.240 eV, as illustrated in Fig. 9. They can be attributed to the LO phonon replicas of free excitons and result from the simultaneous emission of photons and phonons in the annihilation process of free excitons. For the as-deposited film, the PL spectrum taken at 7 K is also dominated by the NBE luminescence arising from free and bound exciton complexes, but the detailed

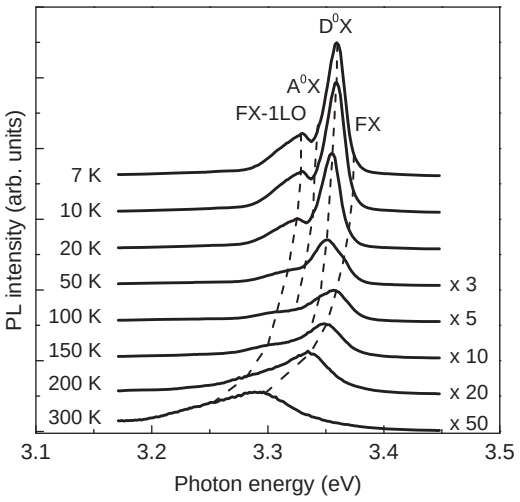

Fig. 10. Temperature dependent PL spectra of nc-ZnO film on Si after annealing at 600 °C.

excitonic features are not so well resolved except for the strongest emission related to the neutral donor bound excitons.

The photo-generated excitons in the nc-ZnO and their evolution with temperature are studied by temperature dependent PL measurements, from which the origin of UV luminescence is also confirmed. Fig. 10 illustrates the PL spectra taken from the annealed nc-ZnO film at temperatures from 7 to 300 K. It can be seen that the exciton emissions of FX, D^0X, and A^0X show obvious redshifts as the sample temperature increases. Meanwhile, the intensity of the UV NBE luminescence decreases as a whole. However, the emission associated with bound excitons decreases more rapidly than that associated with free excitons and becomes hardly resolvable at around 150 K, indicating the decomposition of bound excitons to free ones with increasing thermal energy [33]. The quenching temperature of this emission is lower than that for bulk ZnO crystals at 210 K [28]. The rapid thermal quenching suggests that the excitons are bound very weakly, and hence they must be bound to shallow neutral donors rather than deep ones or acceptors. Furthermore, the larger surface-to-volume ratio in ZnO nanostructure could accelerate the decomposition of bound excitons.

From the PL evolution with temperature obtained by temperature dependent PL measurements, it is clearly seen that the maximum of the PL spectra taken at low temperatures coincides with the emission associated with neutral-donor bound excitons. It is exceeded by the emission associated with free excitons as the temperature increases. The latter becomes the strongest PL feature and dominates the luminescence above 150 K. Such an effect of temperature on the luminescence features obviously indicates that the dominant room-temperature NBE luminescence results from radiative recombination of free excitons.

4. Conclusions

Highly *c*-axis oriented nanocrystalline ZnO thin films with low density of oxygen vacancies were prepared on lattice mismatched Si (100) substrates by the reactive pulsed laser deposition with the assistance of ECR oxygen plasma and post deposition annealing. The oxygen plasma provides sufficient reactive oxygen for the reactive deposition of ZnO with low-density oxygen vacancies and extra energy for the *c*-axis oriented growth of nanocrystalline ZnO at low temperatures. The crystallites grow larger upon thermal annealing together with the improvement in crystallinity. Annealing

temperatures from 600 to 800 °C are most favorable for crystalline perfection of wurtzite ZnO. At excitation by 325 nm light at room temperature, the as-deposited nc-ZnO films emit strong NBE luminescence resulting from radiative recombination of free excitons with a high intensity ratio to the visible DL emission. The PL features are strongly influenced by the annealing process. The ultraviolet emission is greatly enhanced after annealing at temperatures around 800 °C, while higher temperature annealing results in the introduction of oxygen vacancies, and hence a remarkable enhancement of defect related visible emission. Both free and bound exciton associated emissions are observed at low temperatures and show obvious redshifts with increasing measurement temperature together with a decrease of PL intensity. The bound exciton associated emission decreases more rapidly than that associated with free excitons due to the decomposition of bound excitons to free ones with increasing thermal energy. The latter ultimately dominates the NBE emission above 150 K.

Acknowledgments

This work is supported by the National Natural Science Foundation of China under Contract no. 10875029 and the National Basic Research Program of China under Contract no. 2010CB933703.

References

[1] D.C. Look, B. Claflin, Ya I. Alivov, S.J. Park, The future of ZnO light emitters, Physica Status Solidi A 201 (2004) 2203–2212.
[2] K. Ramnathan, M.A. Contreas, C.L. Perkins, S. Asher, F.S. Hasoon, J. Keane, D. Young, M. Romero, W. Metzger, R. Noufi, J. Ward, A. Duda, Properties of 19.2% efficiency ZnO/CdS/CuInGaSe$_2$ thin-film solar cells, Progress in Photovoltaics 11 (2003) 225–230.
[3] M.M. Islama, S. Ishizuka, A. Yamada, K. Matsubara, S. Niki, T. Sakurai, K. Akimoto, Thickness study of Al:ZnO film for application as a window layer in Cu($In_{1-x}Ga_x$)Se$_2$ thin film solar cell, Applied Surface Science 257 (2011) 4026–4030.
[4] S. Fay, L. Feitknecht, R. Schluchter, U. Kroll, E. Vallat-Sauvain, A. Shash, Rough ZnO layers by LP-CVD process and their effect in improving performance of amorphous and microcrystalline silicon solar cells, Solar Energy Materials and Solar Cells 90 (2006) 2960–2967.
[5] M.L. Addonizio, A. Antonaia, Surface morphology and light scattering properties of plasma etched ZnO: B films grown by LP-MOCVD for silicon thin film solar cells, Thin Solid Films 518 (2009) 1026–1031.
[6] M. Dürr, A. Schmid, M. Obermaier, S. Rosselli, A. Yasuda, G. Nelles, Low-temperature fabrication of dye-sensitized solar cells by transfer of composite porous layers, Nature Materials 4 (2005) 607–611.
[7] C.Y. Jiang, X.W. Sun, K.W. Tan, G.Q. Lo, A.K.K. Kyaw, D.L. Kwong, A high-bendability flexible dye-sensitized solar cell with a nanoparticle-modified ZnO-nanowire electrode, Applied Physics Letters 92 (2008) 143101-1–143101-3.
[8] H.W. Chen, C.Y. Lin, Y.H. Lai, J.G. Chen, C.C. Wang, C.W. Hu, C.Y. Hsu, R. Vittal, K.C. Ho, Electrophoretic deposition of ZnO film and its compression for a plastic based flexible dye-sensitized solar cell, Journal of Power Sources 196 (2011) 4859–4864.
[9] K. Wang, J. Chen, W. Zhou, Y. Zhang, Y. Yan, J. Pern, A. Mascarenhas, Direct growth of highly mismatched type II ZnO/ZnSe core/shell nanowire arrays on transparent conducting oxide substrates for solar cell applications, Advanced Materials 20 (2008) 3248–3253.
[10] Z. Wu, Y. Zhang, J. Zheng, X. Lin, X. Chen, B. Huang, H. Wang, K. Huang, S. Li, J. Kang, An all-inorganic type-II heterojunction array with nearly full solar spectral response based on ZnO/ZnSe core/shell nanowires, Journal of Materials Chemistry 21 (2011) 6020–6026.
[11] J. Chen, H. Ye, L. Ae, Y. Tang, D. Kieven, T. Rissom, J. Neuendorf, M.Ch. Lux-Steiner, Tapered aluminum-doped vertical zinc oxide nanorod arrays as light coupling layer for solar energy applications, Solar Energy Materials and Solar Cells 95 (2011) 1437–1440.
[12] K. Ostrikov, Colloquium: reactive plasmas as a versatile nanofabrication tool, Reviews of Modern Physics 77 (2005) 489–511.
[13] J. Shao, Y.Q. Shen, J. Sun, N. Xu, D. Yu, Y.F. Lu, J.D. Wu, Low-temperature *c*-axis oriented growth of nanocrystalline ZnO thin films on Si substrates by plasma assisted pulsed laser deposition, Journal of Vacuum Science & Technology B 26 (2008) 214–218.
[14] K. Gao, W. Zhang, J. Sun, N. Xu, Z.F. Ying, Q. Li, J. Gan, J.D. Wu, Influences of substrate and annealing on the structural and optical properties and photoluminescence of nanocrystalline ZnO films prepared by plasma assisted pulsed laser deposition, Journal of Physical Chemistry C 113 (2009) 19139–19144.
[15] J.Y. Tang, W. Zhang, J. Sun, N. Xu, C. Ge, J.D. Wu, Spectroscopic study on the enhanced excitation of ECR nitrogen plasma by pulsed laser ablation of an aluminum target, Applied Spectroscopy 62 (2008) 1256–1261.
[16] B.D. Cullity, S.R. Stock, Elements of X-ray Diffraction, 3rd ed., Prentice Hall, Englewood Cliffs, NJ, 2001, p. 170.
[17] B.D. Cullity, S.R. Stock, Elements of X-ray Diffraction, 3rd ed., Prentice Hall, Englewood Cliffs, NJ, 2001, pp. 101–103.
[18] M.A. Verges, A. Mifsud, C.J. Serna, Formation of rod-like zinc-oxide microcrystals in homogeneous solutions, Journal of the Chemical Society—Faraday Transactions 86 (1990) 959–963.
[19] M. Asghar, H. Noor, M.S. Awan, S. Naseem, M.A. Hasan, Post-annealing modification in structural properties of ZnO thin films on p-type Si substrate deposited by evaporation, Materials Science in Semiconductor Processing 11 (2008) 30–35.
[20] S. Senthilkumaar, K. Rajendran, S. Banerjee, T.K. Chini, V. Sengodan, Influence of Mn doping on the microstructure and optical property of ZnO, Materials Science in Semiconductor Processing 11 (2008) 6–12.
[21] D.C. Agarwal, R.S. Chauhan, A. Kumar, D. Kabiraj, F. Singh, S.A. Khan, D.K. Avasthi, J.C. Pivin, M. Kumar, J. Ghatak, P.V. Satyam, Synthesis and characterization of ZnO thin film grown by electron beam evaporation, Journal of Applied Physics 99 (2006) 123105-1–123105-6.
[22] C.A. Arguello, D.L. Rousseau, S.P.S. Porto, First-order Raman effects in wurtzite-type crystals, Physical Review 181 (1969) 1351–1363.
[23] T.C. Damen, S.P.S. Porto, B. Tell, Raman effects in zinc oxide, Physical Review 142 (1966) 570–574.
[24] V. Pachauri, C. Subramaniam, T. Pradeep, Novel ZnO nanostructures over gold and silver nanoparticle assemblies, Chemical Physics Letters 423 (2006) 240–246.
[25] C.J. Youn, T.S. Jeong, M.S. Han, J.H. Kim, Optical properties of Zn-terminated ZnO bulk, Journal of Crystal Growth 261 (2004) 526–532.
[26] J.F. Scott, UV resonant Raman scattering in ZnO, Physical Review B 2 (1970) 1209–1211.
[27] D.W. Hamby, D.A. Lucca, M.J. Klopfstein, G. Cantwell, Temperature dependent exciton photoluminescence of bulk ZnO, Journal of Applied Physics 79 (2003) 3214–3217.
[28] W. Shan, W. Walukiewicz, J.W. Ager, K.M. Yu, H. Yuan, H.P. Xin, G. Cantwell, Nature of room-temperature photoluminescence in ZnO, Applied Physics Letters 86 (2005) 191911-1–191911-3.
[29] H.S. Kang, J.W. Kim, S.H. Lim, H.W. Chang, G.H. Kim, J.H. Kim, S.Y. Lee, Investigation on the variation of green, yellow, and orange emission properties of ZnO thin film, Superlattices and Microstructures 39 (2006) 193–201.
[30] K. Vanheusden, W.L. Warren, C.H. Seager, D.K. Tallant, J.A. Voigt, B.E. Gnade, Mechanisms behind green photoluminescence in ZnO phosphor powders, Journal of Applied Physics 79 (1996) 7983–7990.
[31] K. Vanheusden, C.H. Seager, W.L. Warren, D.R. Tallant, J.A. Voiget, Correlation between photoluminescence and oxygen vacancies in ZnO phosphors, Applied Physics Letters 68 (1996) 403–405.
[32] D. Li, Y.H. Leung, A.B. Djurišić, Z.T. Liu, M.H. Xie, S.L. Shi, S.J. Xu, W.K. Chan, Different origins of visible luminescence in ZnO nanostructures fabricated by the chemical and evaporation methods, Applied Physics Letters 85 (2004) 1601–1603.
[33] X.L. Xu, M.J. Zheng, G.D. Ding, W.Z. Shen, Fabrication and optical properties of highly ordered ZnO nanodot arrays, Chemical Physics Letters 411 (2005) 37–42.